

Article

The Origin of the Low-Temperature Minimum of Electrical Resistivity in Strontium Ferromolybdate Ceramics

Gunnar Suchaneck ^{1,*} , Evgenii Artiukh ²  and Gerald Gerlach ¹ ¹ Solid-State Electronics Laboratory, TU Dresden, 01062 Dresden, Germany; gerald.gerlach@tu-dresden.de² Cryogenic Research Division, SSPA “Scientific-Practical Materials Research Centre of NAS of Belarus”, 220072 Minsk, Belarus; sirfranzferdinand@yandex.ru

* Correspondence: gunnar.suchaneck@tu-dresden.de

Abstract: In this work, we analyze the electrical behavior of strontium ferromolybdate below room temperature. We demonstrate that in SFMO ceramics, SFMO thin films deposited by pulsed laser deposition including (100) and (111) textured thin films, as well as in nonstoichiometric SFMO ceramics, an intergrain tunneling mechanism of charge carrier conduction leads to a decrease in resistivity with increasing temperature in the low-temperature region. This intergrain tunneling can be attributed to fluctuation-induced tunneling. On the other hand, bulk metallic resistivity of the grains, which increases with temperature, becomes dominant at higher temperatures and magnetic fluxes. The interplay of these conduction mechanisms leads to a resistivity minimum, i.e., a resistivity upturn below the temperature of minimum resistivity. Several mechanisms have been discussed in the literature to describe the low-temperature upturn in resistivity. Based on available literature data, we propose a revised model describing the appearance of a low-temperature resistivity minimum in SFMO ceramics by an interplay of fluctuation-induced tunneling and metallic conductivity. Additionally, we obtained that in the region of metallic conductivity at higher temperatures and magnetic fluxes, the pre-factor R_m of the temperature-dependent term of metallic conductivity written as a power law decreases exponentially with the temperature exponent m of this power law. Here, the value of m is determined by the charge scattering mechanism.

Keywords: strontium ferromolybdate; electrical resistivity; low-temperature electrical behavior

Citation: Suchaneck, G.; Artiukh, E.; Gerlach, G. The Origin of the Low-Temperature Minimum of Electrical Resistivity in Strontium Ferromolybdate Ceramics. *Ceramics* **2024**, *7*, 491–503. <https://doi.org/10.3390/ceramics7020032>

Academic Editors: Dawei Wang and Fayaz Hussain

Received: 12 February 2024

Revised: 19 March 2024

Accepted: 28 March 2024

Published: 1 April 2024



Copyright: © 2024 by the authors. Licensee MDPI, Basel, Switzerland. This article is an open access article distributed under the terms and conditions of the Creative Commons Attribution (CC BY) license (<https://creativecommons.org/licenses/by/4.0/>).

1. Introduction

Strontium ferromolybdate ($\text{Sr}_2\text{FeMoO}_{6-\delta}$, SFMO) double perovskites are promising candidates for magnetic electrode materials for room-temperature spintronic applications, because they have a half-metallic character (with theoretically 100% electron spin polarization), present a high Curie temperature of about 420 K (magnets should be operated in their ordered magnetic state below Curie temperature), and show a low-field magnetoresistance [1].

Modern artificial intelligence (AI) text generators such as ChatGPT are based on neural networks. The conventional complementary metal–oxide–semiconductor (CMOS) neuron and synapse designs require numerous transistors and feedback mechanisms and would be unsuitable for developing modern AI systems. Since the early developments of neural network theory, magnetic materials have been used for modeling brain-like systems. The main advantage of spintronics compared to other resistive memories for neuromorphic computing is the possibility to induce complex and tunable resistance dynamics through spin torque. Like other memory cells, they can switch between two fixed states, allowing them to emulate synapses. Thus, neuromorphic spintronics aims to develop spintronic hardware devices and circuits with brain-inspired principles [2], i.e., spintronics is a promising approach to neuromorphic computing as it potentially enables energy-efficient and area-efficient embedded applications by mimicking key features of

biological synapses and neurons with a single device instead of using multiple electronic components [3,4].

The main reasons for the still missing wide application of SFMO is the low reproducibility of its electrical and magnetic properties originating in the formation of point defects and grain boundaries with a composition different from the bulk of the grains, as well as its aging in contact with air and moisture.

The charge transport mechanisms of perovskites are strongly dependent on synthesis conditions and, thus, on the microstructure of the material (single-crystalline, polycrystalline, grain size, nature of grain boundaries, and others) formed by its synthesis. SFMO ceramics obtained by solid-state reactions using one and the same procedure were insulating, metallic, or in an intermediate state in dependence on the precursors and annealing temperature and time [5]. In SFMO, the transport properties are dominated by spin-polarized intergrain tunneling through insulating grain boundaries [6]. Therefore, the transport properties will be different in ceramics, thin films, and single crystals. Single crystals possess a 4 mm symmetry while ceramics have a ∞ m one. Columnar thin films will be in an intermediate state between 4 mm and ∞ m symmetry. Consequently, the interpretation of grain size parameters will be very different for each of these structures. Under specific synthesis conditions, SFMO ceramics consist of SrMoO₄ (SMO) intergrain energy barriers between conductive bulks of SFMO grains induced by a small oxygen excess during material fabrication [7]. Previously, we have shown that an appropriate thermal treatment leads to the formation of dielectric SrMoO₄ shells at the surface of SFMO nanograins. The formation of thin insulating SrMoO₄ surface layers suppresses the metallic conductivity owing to the appearance of intergrain fluctuation-induced tunneling [8]. The ease of forming SMO shells around SFMO grains during synthesis simply by excess oxygen during synthesis makes SFMO an easy-to-fabricate, natural core-shell material.

Generally, several mechanisms have been discussed to interpret the low-temperature resistivity upturn that was visible in experiments: (i) inelastic scattering of electrons by impurity ions in impure metals [9], (ii) Kondo-like effects associated with dilute magnetic impurities in a nonmagnetic host [10–14], (iii) quantum interference effects arising from electron–electron interactions and weak localization [15–22], (iv) electron–electron interaction driven by Coulomb forces in a strongly correlated system [23], (v) spin-polarized tunneling via grain boundaries in ceramic manganites [24], (vi) the competition of two mechanisms—one contribution decreasing with temperature combined with another contribution increasing with temperature [10,25], and (vii) two spin channels in SFMO connected in parallel, where the spin-down channel is metallic (with a non-zero density of states at the Fermi level), and the spin-up channel (with a gap in the band structure) behaves like a semiconductor [26].

Several reports have considered an interplay of two mechanisms or a crossover between them [13,16,27]. However, a satisfactory description has not yet emerged and is still under discussion.

The Kondo effect mentioned above was discovered by Jun Kondo in 1964 [10]. It describes the scattering of conduction electrons in a metal due to the resonant interaction between conduction charge carriers and the spin of localized magnetic impurity ions. Kondo applied third-order perturbation theory to the problem of scattering of s-orbital conduction electrons by d-orbital electrons localized at impurities. Kondo's approach predicted a logarithmical increase in the scattering rate and the resulting part of the resistivity as the temperature approaches absolute zero. This results in an anomalous upturn in resistivity at low temperatures. Thereby, the steepness of the upturn is proportional to the impurity concentration. Considering an Fe³⁺-O-Fe⁴⁺ Kondo lattice in SFMO [28], the resistivity upturn, which occurs in polycrystalline SFMO ceramics in the absence of a magnetic field [29], was reproduced. However, the authors in [28] took into account only four data points of [29]. Considering all data points of [29], the agreement with the experimental data above 240 K would become worse. In La_{2/3}Sr_{1/3}MnO₃, the Kondo resistivity contributions are expected to collapse at a magnetic flux density of about 13 T [27]. We excluded the Kondo effect

as a possible cause since a frustrated spin-glass-like structure is present at the surfaces of weakly connected ferromagnetic grains in cold-pressed polycrystalline SFMO [30]. In this case, the spin degrees of freedom are completely frozen and, thus, internal degrees of freedom are absent. The frustrated spin-glass structure leads to a strong exchange bias effect, which is seen in the field-cooled magnetoresistance measurements [31]. Here, the presence of a high field irreversibility starting below 235 K between the field-cooled and zero-field-cooled curves at a magnetic flux of 1 T is attributed to a possible spin-glass component at the distorted surfaces of nanoparticles obtained earlier in NiFe₂O₄ [32] and La_{2/3}Sr_{1/3}MnO₃ [33]. Other signatures for a frustrated spin-glass structure are a wider hysteresis in magnetoresistance compared to that in magnetization [34,35] and the shift of the low-temperature peak of the imaginary part of AC susceptibility to higher temperatures with the increase in frequency [35,36].

Weak localization is a physical effect, which occurs in disordered electronic systems at very low temperatures. The origin of weak localization is quantum interference of back-scattered electrons. The effect manifests itself as a correction, $\Delta\sigma$, to the conductivity (or correspondingly the resistivity) of a metal or semiconductor arising in the case that the mean free path l is in the order of the Fermi wavelength $\lambda_F = 2\pi/k_F$ of the carrier wave functions with k_F denoting the Fermi wave vector, i.e., $k_F l \sim 1$. Calculations of k_F were carried out assuming an electron density of $n_e = 1.1 \times 10^{22} \text{ cm}^{-3}$ [37], yielding $k_F = (3\pi n_e)^{1/3} = 4.7 \times 10^9 \text{ m}^{-1}$ and $\lambda_F = 0.913 \text{ nm}$. The experimentally obtained low-temperature mean free path amounts to $l(4 \text{ K}) = 1.11 \text{ nm}$ [38] (p. 72), in good agreement with a value of $l = \hbar k_F / n_e e^2 \rho_0 = 0.975 \text{ nm}$ where \hbar is the Planck constant expressed in J s radian⁻¹ and ρ_0 the residual resistivity amounting to $\rho_0 = 1.8 \times 10^{-6} \Omega \text{ m}$ [39]. A strong magnetic field suppresses the contribution of weak localization [16]. In La_{2/3}Sr_{1/3}MnO₃ thin films consisting of ZrO₂ nanoparticles, weak localization vanishes at about 9 T [27]. In ferromagnetic systems, including also ferrimagnetic SFMO, the nuclei already experience a magnetic field without applying any external magnetic field. This is the hyperfine field created by the electrons at the nuclei [40]. It describes the hyperfine interaction between the magnetic moment of the nucleus and the magnetic moment of the electrons in the solid. In SFMO, the hyperfine magnetic field amounts to about 30 T [41]. Thus, weak localization may be excluded from consideration. Recently, we claimed the absence of weak localization in SFMO since fluctuation-induced tunneling as well as adiabatic small polaron hopping do not favor quantum interference. We concluded that the resistivity upturn behavior of SFMO cannot be explained by weak localization [17].

The contribution of electron–electron interactions to the conductivity is similar to that due to weak localization. In this case, the inelastic diffusion length should be replaced by the thermal diffusion length $L_T = (\hbar D / kT)^{1/2}$ and the coefficients are slightly modified [42]. Therefore, the large hyperfine magnetic field will also erase the electron–electron interaction correction to resistivity. In La_{2/3}(Sr,Ca)_{1/3}MnO₃ epitaxial thin films deposited on a (001) LaAlO₃ substrate where the appearance of a resistivity minimum was attributed to the electron–electron interaction of the strongly correlated system, the resistivity upturn below the temperature of minimum resistivity T_{min} was largely unaffected by externally applied fields up to 8 T. This is contrary to data of polycrystalline SFMO ceramics [29].

Spin-polarized intergrain tunneling in manganites was discovered by Hwang et al. in 1996 [43]. The low-temperature resistivity minimum obtained in ceramic manganites was found to explain charge carriers' tunneling between antiferromagnetically coupled grains [21]. The tunneling resistance between two FM grains was described by the theory of tunneling conduction through the FM metal/nonmagnetic barrier/FM metal (fbf) junction using the phenomenological expression [44]

$$\rho(T, B) = \frac{\rho_{\text{fbf}}}{1 + P^2 \langle \cos \theta_{ij} \rangle}, \quad (1)$$

where P is the degree of the spin polarization of the current carriers and θ_{ij} is the angle between the magnetization directions of the grains i and j :

$$\cos \theta_{ij} \Big|_{B=0} = -L(|J|/kT). \quad (2)$$

Here, $L(x) = \coth(x) - 1/x$ is the Langevin function and J the antiferromagnetic interaction constant. Since the temperature dependence of the in-grain and grain boundary magnetization is dominated by the spin-wave $T^{3/2}$ terms at low temperatures, ρ_{fbf} was taken as

$$\rho_{fbf} = \rho_0 + \rho_{1.5}T^{1.5}, \quad (3)$$

where ρ_0 and ρ_1 are parameters independent of B . The model parameters are then defined from the requirement that in the case $B = 0$, Equation (1) fits the experimental data for $\rho(T, B = 0)$ in the range 4.3–50 K. For $\text{La}_{0.5}\text{Pb}_{0.5}\text{MnO}_3$, the fitting parameters that reflect the behavior of the experimentally obtained resistivity minimum were $P = 0.697$, $|J|/k = 155$ K, $\rho_0 = 1.45 \times 10^{-3} \Omega\text{m}$, and $\rho_{1.5} = 1.026 \times 10^{-6} \Omega\text{mK}^{-3/2}$. In the case of SFMO, the parameter $|J|/k$ is significantly lower than for manganites amounting to 47.6 K [37]. This considerably lowers the depth of the resistivity minimum. Also, the resistivity parameters $\rho_0 = 2 \times 10^{-6} \Omega\text{m}$ [39] and $\rho_{1.5} \approx 3 \times 10^{-6} \Omega\text{mK}^{-3/2}$ (estimated below) are different, leading to a curve that increases with temperature. A resistivity minimum is obtained only in the parameter range $\rho_1 \approx 1.5\text{--}8 \times 10^{-9} \Omega\text{mK}^{-3/2}$, which does not correspond to experimental data. Therefore, we disregard spin-polarized tunneling as the origin of the resistivity minimum.

Spin-polarized tunneling between antiferromagnetically coupled grains in ceramic manganites causes a resistivity upturn, which shifts to lower temperature with an increasing magnetic field and disappears above a critical field value amounting to 1.5 T for $\text{La}_{0.5}\text{Pb}_{0.5}\text{MnO}_3$ [24]. The application of a magnetic field increases the probability of electron tunneling through dielectric grain boundaries, thus decreasing the resistivity and recovering the metallic conductivity of the nanograins. This leads to a decrease in the upturn temperature as obtained for SFMO in [29]. It decreases from 180 K at 0.2 T to about 40 K at 7 T. Since the low-field magnetoresistance in polycrystalline perovskites is governed by spin-polarized tunneling across grain boundaries [43], this provides a sufficient low-field magnetoresistance promising for device application [1].

The decrease in the temperature T_{min} of minimum resistivity with an increasing magnetic field also corresponds to the predictions of a model consisting of a series connection of elastic and inelastic scattering mechanisms [21]. The elastic contribution was assumed to arise from the scattering of holes by magnons without a spin flip whereas the inelastic contribution was calculated as quantum correction to resistivity, taking the inverse of the total scattering length as the geometric mean of the inverse phase coherence length and the inverse magnetic length. We have analyzed the disappearance of the resistivity upturn in SFMO with increasing magnetic flux density from resistivity data of polycrystalline SFMO ceramics taken from [29]. Here, an exponential law, $T_{min} \propto B^{-0.4}$, appeared, which is unsuitable for defining a critical magnetic field.

An example of the competition of two resistivity contributions with opposite temperature dependencies is on one hand thermally activated hopping and on the other hand excitation to the mobility edge [45] proposed for $\text{La}_{1-x}\text{Sr}_x\text{MnO}_3$ [46]. For SFMO, another model was considered consisting of a semiconductor-like thermally activated resistivity in one spin channel in parallel to metallic conductivity in the other spin channel [26].

In this work, we propose a modified model describing the appearance of a low-temperature resistivity upturn in SFMO ceramics by an interplay of two conductivity mechanisms: (i) fluctuation-induced tunneling and (ii) metallic conductivity. It is based on the thorough analysis and evaluation of literature data of conductivity behavior of SFMO.

2. Materials and Methods

The resistivity of SFMO thin films produced by pulsed laser deposition below 30 K increases strictly logarithmically with decreasing temperature [38] (p. 64). Such a behavior may be attributed either to the Kondo effect, weak localization, or electron–electron

interaction [14]. However, we have ruled out all these mechanisms for strontium ferromolybdate above.

Near room temperature, two possible conduction mechanisms of nano-sized granular SFMO were obtained that cannot be distinguished by experimental data [8]. The first one is the Mott variable-range hopping describing a carrier transport in a disordered semiconductor or in an amorphous solid by charge carrier hopping between two spatially separated states in an extended temperature range [45]. For three-dimensional conductance when the Coulomb interaction between the carrier is negligible, the resistivity has a characteristic temperature dependence of

$$\rho(T) = \rho_0 \exp\left(\frac{T_0}{T}\right)^{1/4}, \quad (4)$$

with a characteristic temperature T_0 in the order of a few 10^6 K. The value of T_0 defines the hopping activation energy and the mean hopping distance. Alternatively to Mott variable-range hopping, the conductivity in this temperature region may be modeled by a $\ln\rho \propto T^{-1/2}$ dependence derived for (i) two-dimensional conductance in the Mott variable-range hopping model [45]; (ii) Efros–Shklovskii variable-range hopping, which accounts for the Coulomb gap interaction of electrons in localized states that results in the creation of the Coulomb gap near the Fermi energy [47]; or (iii) the low-field conductivity of fine metallic particles dispersed in a dielectric matrix [48]. Note that at higher temperatures, the Coulomb gap can be disregarded and Mott's variable-range hopping comes into effect.

Above room temperature, the resistivity of SFMO ceramics annealed in a vacuum was separated into three regions [49]: (i) from 300 K up to the Curie temperature of about 405 K where the electrical resistivity increases with temperature characteristic for metallic behavior; (ii) above 405 K up to approximately 590 K where resistivity decreases with temperature, which is attributed to a B-site disorder-induced weak Anderson localization of the electrical carriers; and (iii) from 590 K up to 900 K where the resistivity of the material becomes metallic again. On the other hand, the decrease in resistivity in SFMO above the resistivity maximum around Curie temperature was attributed to adiabatic small polaron hopping [17] and not to localization effects as originally suggested [49].

Another report of the electrical resistivity of SFMO [50] indicates metallic conduction behavior below 420 K, the localization of the carriers in the temperature range 420–820 K, and reversion to metallic conduction behavior between 820 K and 1120 K.

In the absence of a magnetic field, the temperature dependence of the conductivity of SFMO ceramics [29] was well described by the fluctuation-induced tunneling (FIT) model [51], e.g., by the presence of conducting grains separated by nano-sized energy barriers where large thermal voltage fluctuations occur when the capacitance of an intergrain junction is in the order of 0.1 fF. Nano-sized energy barriers with a barrier width of a few nanometers and a barrier area of several hundred square micrometers usually occur at grain surfaces in cold-pressed ceramics or ceramics thermally treated under oxidation conditions.

Below 500 K, monocrystalline, half-metallic SFMO exhibits a resistivity, $\rho(T)$, increasing with temperature as

$$\rho(T) = \rho_0 + R_1 T^l, \quad (5)$$

where $\rho_0 = 1.8 \times 10^{-6} \Omega\text{m}$ is the residual metallic resistivity, $l = 2$ near room temperature and $R_2 = 2.16 \times 10^{-11} \Omega\text{mK}^{-2}$ [37,39]. A low-temperature upturn of the resistivity is missing in single-crystal SFMO due to the absence of intergrain boundaries characteristic for ceramics. The T^2 dependence suggests that resistivity is dominated by either electron–electron scattering [39,52] or spin-wave scattering [39]. At higher temperatures up to the Curie temperature T_C , other charge scattering mechanisms come into play that can be considered in Equation (1) by additional terms:

$$\rho(T) = \rho_0 + R_2 T^2 + \sum_l R_l T^l. \quad (6)$$

A term with $l = 2.5$ represents the combination of electron–electron, electron–phonon, and electron–magnon scattering [53], an $l = 3$ term stands for the scattering with anomalous single magnons in half-metallic systems [54], an $l = 3.5$ one stands for the scattering with spin-waves for low temperatures [55,56], and an $l = 4.5$ term describes electron–magnon scattering. The latter was derived in the double-exchange theory at low temperatures [57] but was experimentally observed at elevated temperatures of 200–350 K [52]. Alternatively, the $l = 4.5$ term was attributed to spin-wave scattering [58]. An $l = 5$ term was attributed to acoustic phonon scattering [59]. Additionally, there is a term related to optical phonon scattering:

$$\rho(T) \propto \frac{\omega_s}{\sinh^2(\hbar\omega_s/2kT)}, \quad (7)$$

where ω_s is the average frequency of the softest optical mode, which is consistent with small polaron coherent motion involving relaxation [60], and k is the Boltzmann constant.

Unfortunately, none of these models fit to the experimental data of SFMO thin films in the whole temperature range. However, according to [26], the electron–electron scattering model seems to be appropriate in a broader temperature range. In general, the metallic resistivity of SFMO can be modeled by the equation

$$\rho(T) = \rho_0 + R_m T^m, \quad (8)$$

where m is a fitting parameter that represents an averaged value of the above-mentioned contributions of charge scattering mechanisms characterized by the parameter l .

The FIT model describes conducting grains separated by energy barriers that are subjected to large thermal fluctuations, e.g., carbon-polyvinylchloride composites, consisting of aggregates of carbon spheres [51]. The tunneling occurs between large metallic grains across insulating barriers with width w and area A . It is specified by two parameters, temperature T_1 and a normalized temperature, T_0 . T_1 characterizes the electrostatic energy of a parabolic potential barrier:

$$kT_1 = \frac{A \cdot w \cdot \epsilon_0 E_0^2}{2}. \quad (9)$$

Here, ϵ_0 is the vacuum permittivity. The characteristic electric field strength E_0 is determined by the barrier height V_0 :

$$E_0 = \frac{4V_0}{e \cdot w}. \quad (10)$$

with e the electron charge. The normalized temperature T_0 relates T_1 to the tunneling constant:

$$T_0 = T_1 \cdot \left(\frac{\pi\chi w}{2} \right)^{-1}, \quad (11)$$

with the reciprocal localization length of the wave function

$$\chi = \sqrt{\frac{2m_e V_0}{\hbar^2}}, \quad (12)$$

where m_e is the electron mass. The resulting electrical conductivity in this model is then given by [51]:

$$\sigma(T) = \sigma_{0,FIT} \exp\left(-\frac{T_1}{T_0 + T}\right). \quad (13)$$

Note that the original derivation of Equation (13) considers conductivity, meaning the inverse of resistivity. For SFMO, the characteristic field strength E_0 of the fluctuation-induced tunneling model is nearly independent of temperature and amounts to $4.07 \times 10^4 \text{ Vm}^{-1}$ [61], while V_0 is in the order of 10 meV and w in the range of 1–3 nm [8,61]. Equation (13) demonstrates that the FIT model links the temperature-independent tunnel-

ing conductivity [62] with a temperature-dependent conductivity obtained for tunneling of spin-polarized electrons in granular metal films [63]. The FIT model was recently applied to intergrain tunneling in polycrystalline SFMO ceramics [64], in half-metallic double-perovskite $\text{Sr}_2\text{BB}'\text{O}_6$ ($\text{BB}' = \text{FeMo}, \text{FeRe}, \text{CrMo}, \text{CrW}, \text{CrRe}$) ceramics [65], in $\text{Ba}_2\text{FeMoO}_6$ thin films [66], and in nano-sized SFMO ceramics fabricated by the citrate-gel technique [8]. Surprisingly, we obtained recently [17] that the FIT model satisfactorily describes conductivity behavior of polycrystalline SFMO ceramics in the absence of a magnetic field [29]. In this work, we extend this analysis to other literature data and include the presence of a magnetic field.

3. Results and Discussion

In [26], SFMO was considered as a system with two spin channels connected in parallel. The spin-down channel is metallic and the spin-up channel with a gap in the band structure behaves like a semiconductor. The band gap of the SFMO spin-up band is small enough so that the temperature can excite electrons to the conduction band. The total resistivity is formed by the resistivity of the semiconductive spin channel including some residual resistivity from impurities as well as defects and the resistivity of the metallic spin channel. The E_g values reported in [26] were less than 10 meV, except for a film with higher saturation magnetization with $E_g = 47.3$ meV. The latter was deposited at slightly higher pressure (11 Pa compared to 9 Pa) and in a more oxidizing atmosphere with a reduced 5% H_2/Ar flow. These E_g values are significantly smaller than the majority of spin-up band gap in SFMO, amounting to about 0.8 eV [67]. They are in the order of the parameter Δ describing the spin-dependent tunneling for Co-Al-O insulating granular film [68] and lie in the order of the barrier V_0 of fluctuation-induced tunneling [8,61]. Therefore, we postulate that the low-temperature conductivity mechanism with high probability originates from intergranular tunneling. In contrast, the conductivity at mediate temperature can be attributed to metallic conductivity.

In the following, we will consider a brick model consisting of cube-shaped grains with metallic conductivity covered at the surface by grain boundaries creating nano-sized intergrain tunneling barriers. Here, two types of grain boundaries appear, namely one with a normal vector parallel to the applied field (perpendicular boundaries) and another one with a normal vector perpendicular to the applied field (parallel boundaries). The corresponding DC equivalent circuit is an intragrain resistance in parallel with the intergrain resistance of parallel grain boundaries and a series connection of this parallel circuit with the intergrain resistance of perpendicular grain boundaries [69]. In our case, the series intergrain resistance of perpendicular grain boundaries may be neglected since—with regard to a very small barrier height in the order of 10 meV—a bias of already a few mV sufficiently increases the tunneling current and, thus, decreases the barrier resistance. Contrarily, the resistance of parallel boundaries remains high since the normal vector of the grain boundary is along an equipotential line. Following [69], we obtain a temperature-dependent conductivity of

$$\sigma(T) = [\rho_0 + R_m T^m]^{-1} + \frac{2w}{d} \sigma_{0,FIT} \exp\left(-\frac{T_1}{T_0 + T}\right), \quad (14)$$

where w is the barrier width and d the grain size amounting for nano-sized SFMO ceramics fabricated by the citrate-gel method; $w = 1.24$ nm and $d = 75$ nm [8]. Unfortunately, only a few publications provide values of both w and d . When matching the FIT model and metallic conductivities, the inverse of the metallic residual resistivity corresponds to the FIT model conductivity for temperature and barrier height tending to zero. Thus, we introduce for the sake of simplicity an effective model resistivity, $\rho_0 = 1/\sigma_{0,FIT}$, which is valid for $2w/d \approx 1$. In the following, we are considering a resistivity minimum arising from the competition of two contributions, one of which is fluctuation-induced tunneling dominating the resistivity at low temperatures and low magnetic fields and the other one is metallic conductivity leading to a growing conductivity with increasing temperature. To

confirm this, we will now analyze available literature data with respect to the parameters of electrical conductivity. Figure 1 shows resistivity data of polycrystalline SFMO ceramics fabricated by the solid-state reaction technique [29]. The solid lines are curves fitting these data to the model of this work, Equation (14). Table 1 compiles the model parameters of various SFMO materials. Corresponding fits for SFMO thin films deposited by pulse laser deposition are depicted in Figure 2.

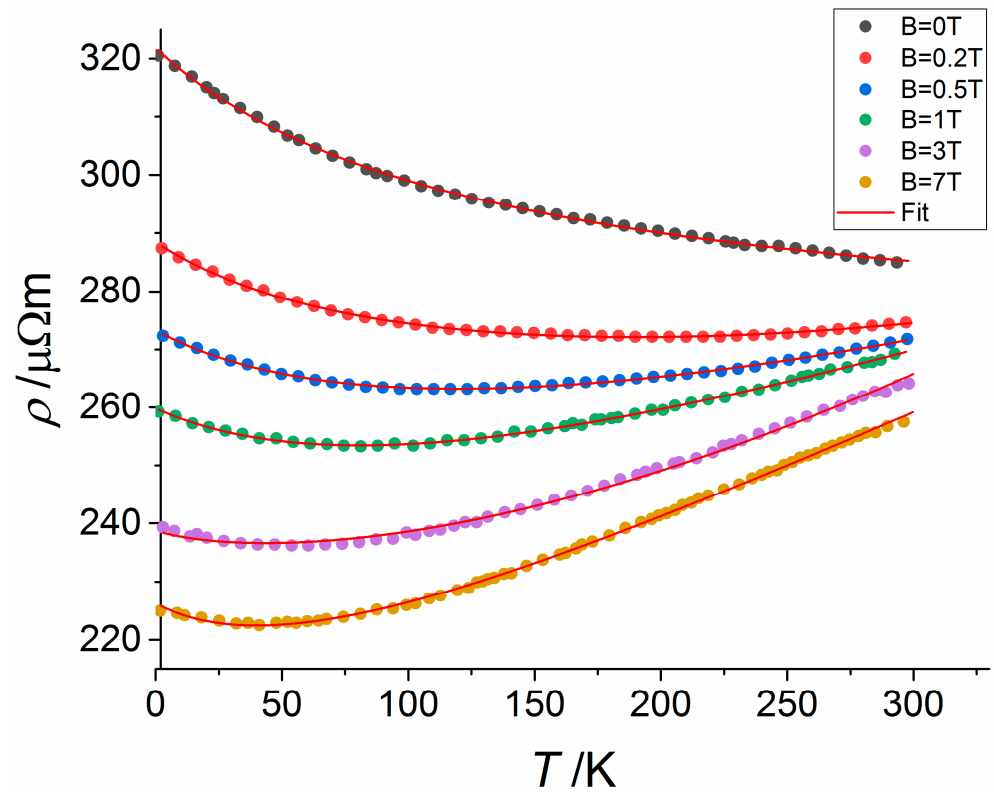


Figure 1. Fit of resistivity data of polycrystalline SFMO ceramics fabricated by the solid-state reaction technique [29] to Equation (14).

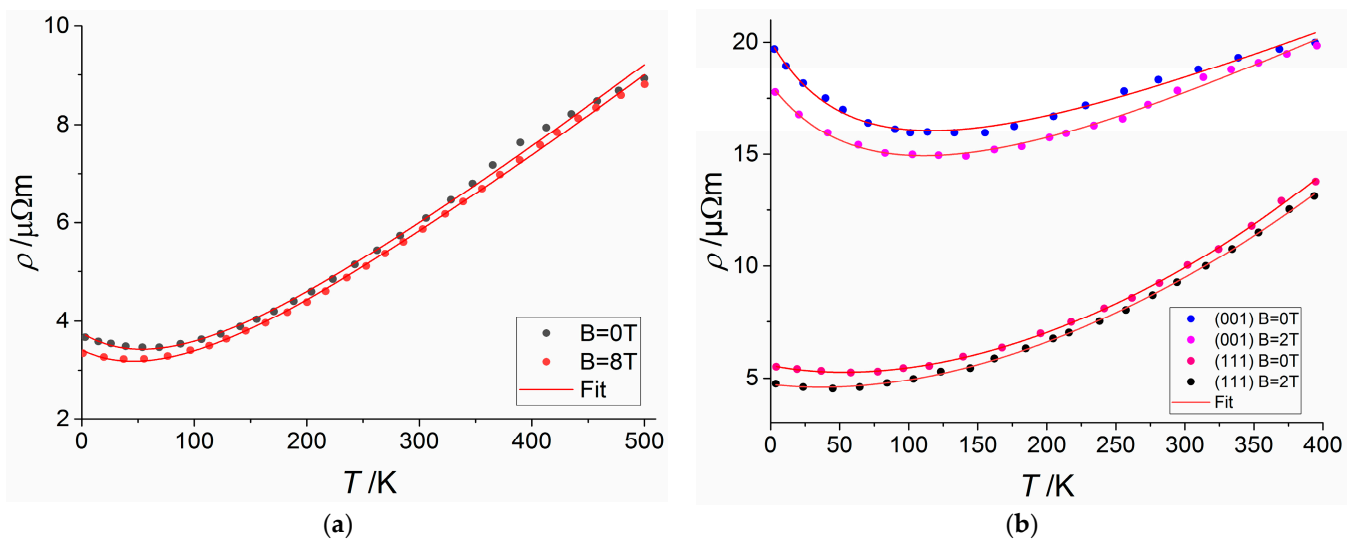


Figure 2. Fit of resistivity data (a) from [71] and (b) from [73] of ordered SFMO thin films deposited by pulsed laser deposition to Equation (14).

Table 1. Fit parameters for Equation (14) of various SFMO materials.

SFMO Material	B, T	T ₁ , K	T ₀ , K	1/ρ ₀ , S/m	m	R _m , ΩmK ^{-m}	Ref.
Sintered ¹ polycrystalline SFMO ceramics	0	362.2	180.7	0.28	1.24	7.84 × 10 ⁻⁴	[29]
	0.2	341.9	102.5	0.34	1.41	5.13 × 10 ⁻⁴	
	0.5	265.4	67.7	0.36	1.44	6.50 × 10 ⁻⁴	
	1	323.7	77.6	0.38	1.59	2.43 × 10 ⁻⁴	
	3	362.3	75.5	0.42	1.75	9.82 × 10 ⁻⁵	
SFMO ceramics ¹	7	323.1	62.0	0.44	1.80	9.28 × 10 ⁻⁵	[70]
	0	1541.7	492.6	14.6	3	1.19 × 10 ⁻⁹	
Thin film ²	0	1272.5	509.3	26.0	2.72	9.76 × 10 ⁻⁹	[71]
	8	2003.8	831.6	28.2	2.40	5.20 × 10 ⁻⁸	[71]
Thin film ²	0	88.0	84.5	42.1	2.9	1.93 × 10 ⁻⁹	[72]

¹ Sintered 2 h at 1200 °C in 1 % H₂/Ar, ² deposited by pulse laser deposition.

Figure 3 demonstrates that model Equation (14) is also valid for the data of ordered, nonstoichiometric SFMO ceramics prepared by a solid-state reaction at 900 °C and sintered at 1280 °C for 12 h in a stream of 5% H₂/Ar [74].

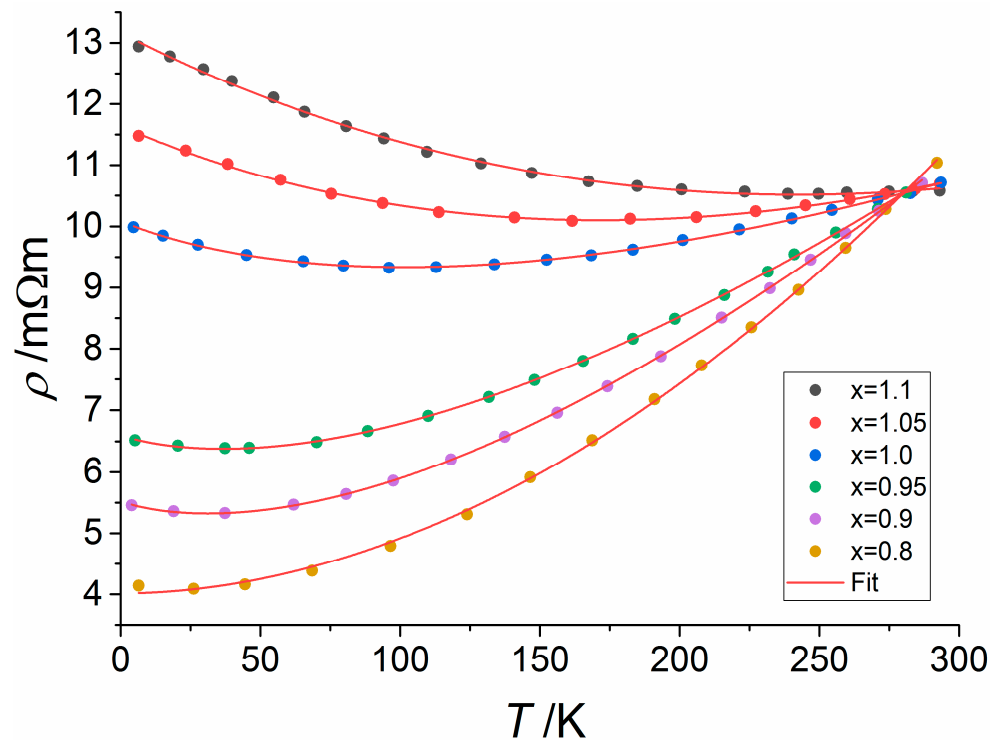


Figure 3. Fit of resistivity data from [74] of nonstoichiometric Sr₂Fe_xMo_{2-x}O₆ ceramics prepared by solid-state reaction and sintered for 12 h at 1280 °C in a stream of 5% H₂/Ar to Equation (14).

The ratio T₁/T₀ defines a value of the product χw of the reciprocal localization length of the wave function χ and barrier width w. Since the value of the tunnel barrier height V₀ depends on the nature and configuration of chemical bonds in the intergrain area, the differences in V₀ for different SFMO materials should be small. For given values of V₀, the value of χ can be calculated by means of Equation (12). The barrier width w then defines T₁/T₀ via Equation (11). In the first case, the magnetic flux dependence on V₀ should be taken into account that follows the relation [75]

$$V_0(B) = V_0(0) - \beta B + \gamma B^2 \tag{15}$$

with β = 1.16 meV/T and γ = 0.04 meV/T² [76]. This results in a ratio, T₁/T₀, that decreases slightly as the magnetic flux increases. This is in qualitative agreement with the ratios T₁/T₀

derived from experimental data [71,73] (cf. Table 1). On the other hand, this contradicts the data derived from [29], where T_1/T_0 increases with magnetic flux.

For metallic conductivity, the values of R_m and m in Equation (8) are correlated [77]. In our case, this is illustrated in Figure 4, showing an exponential decrease in R_m with m . Note that Figure 4 yields for $m = 1.5$ a value of $\rho_{1.5} \approx 3 \times 10^{-6} \Omega\text{mK}^{-3/2}$ which is required in Equation (3).

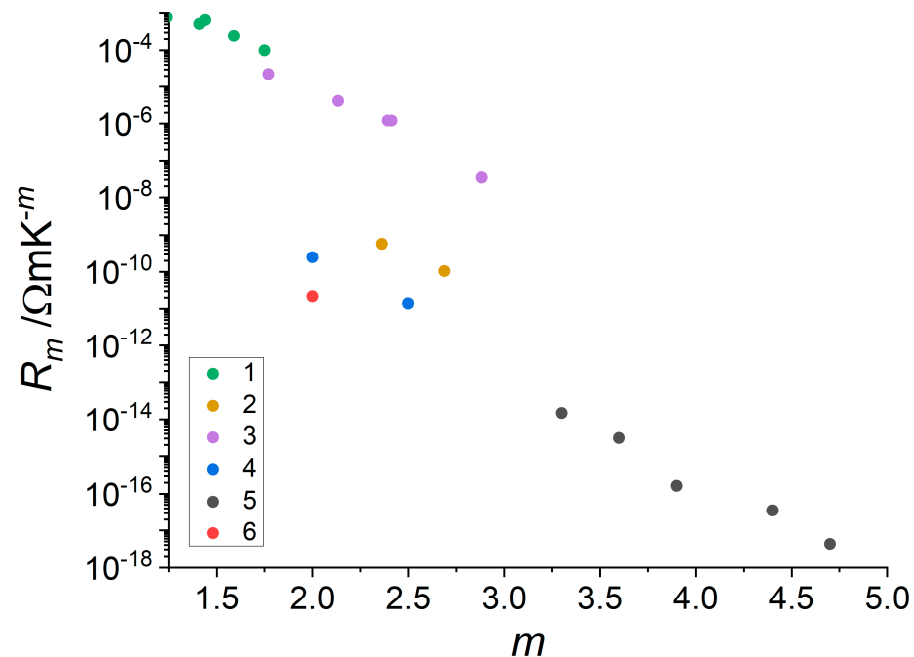


Figure 4. Correlation between pre-factor R_m and exponent m in Equation (8). 1—[29], 2—[71], 3—[74], 4—[77], 5—[78], 6—[79].

4. Conclusions

In this work, we propose a novel explanation of the low-temperature resistivity minimum in ceramic strontium ferromolybdate ceramics possessing nano-sized intergrain barriers that is in agreement with given experimental data from various publications. According to our findings, the resistivity upturn is not caused by a semiconductor–metallic transition, but it can be attributed to intergrain fluctuation-induced tunneling dominating at low temperatures the conductivity of the considered SFMO ceramics. Based on known analytical approaches, a modified model, Equation (14), of the total conductivity of granular ceramics was derived. This model is shown to be valid for cold-pressed SFMO ceramics as well as SFMO ceramics thermally treated under oxidation conditions, SFMO thin films deposited by pulsed laser deposition including (100) and (111) textured thin films, and nonstoichiometric SFMO ceramics. In the region of metallic conductivity at elevated temperatures and higher magnetic fluxes, the pre-factor R_m of the temperature-dependent term of metallic conductivity written as a power law decreases exponentially with the exponent m of this power law. Here, the value of m is determined by the charge scattering mechanism.

Author Contributions: Conceptualization, G.S.; methodology, G.S.; software, E.A.; validation, E.A. and G.G.; formal analysis, E.A.; investigation, G.S. and E.A.; resources, G.G.; data curation, E.A.; writing—original draft preparation, G.S.; writing—review and editing, E.A. and G.G.; visualization, E.A.; supervision, G.G.; project administration, G.S. and G.G.; funding acquisition, G.S. and G.G. All authors have read and agreed to the published version of the manuscript.

Funding: This work was funded by the EU project H2020-MSCA-RISE-2017-778308-SPINMULTIFILM.

Institutional Review Board Statement: Not applicable.

Informed Consent Statement: Not applicable.

Data Availability Statement: The original contributions presented in the study are included in the article; further inquiries can be directed to the corresponding author.

Conflicts of Interest: The authors declare no conflicts of interest.

References

- Suchanec, G.; Kalanda, N.; Artsiukh, E.; Gerlach, G. Challenges in $\text{Sr}_2\text{FeMoO}_{6-\delta}$ thin film deposition. *Phys. Status Solidi B* **2020**, *257*, 1900312. [[CrossRef](#)]
- Grollier, J.; Querlioz, D.; Stiles, M.D. Spintronic nanodevices for bioinspired computing. *Proc. IEEE* **2024**, *104*, 2024–2039. [[CrossRef](#)] [[PubMed](#)]
- Mishra, R.; Kumar, D.; Yang, H. Oxygen-migration-based spintronic device emulating a biological synapse. *Phys. Rev. Appl.* **2019**, *11*, 054065. [[CrossRef](#)]
- Zhou, J.; Zhao, T.; Shu, X.; Liu, L.; Lin, W.; Chen, S.; Shi, S.; Yan, X.; Liu, X.; Chen, J. Spin-orbit torque-induced domain nucleation for neuromorphic computing. *Adv. Mater.* **2021**, *33*, 2103672. [[CrossRef](#)] [[PubMed](#)]
- Chmaissem, O.; Kruk, R.; Dabrowski, B.; Brown, D.E.; Xiong, X.; Kolesnik, S.; Jorgensen, J.D.; Kimball, C.W. Structural phase transition and the electronic and magnetic properties of $\text{Sr}_2\text{FeMoO}_6$. *Phys. Rev. B Condens. Matter Mater. Phys.* **2000**, *62*, 14197–14206. [[CrossRef](#)]
- Kim, T.H.; Uehara, M.; Cheong, S.-W.; Lee, S. Large room-temperature intergrain magnetoresistance in double perovskite $\text{SrFe}_{1-x}(\text{Mo or Re})_x\text{O}_3$. *Appl. Phys. Lett.* **1999**, *74*, 1737–1739. [[CrossRef](#)]
- Niebieskikwiat, D.; Caneiro, A.; Sánchez, R.D.; Fontcuberta, J. Oxygen-induced grain boundary effects on magnetotransport properties of $\text{Sr}_2\text{FeMoO}_{6+\delta}$. *Phys. Rev. B Condens. Matter Mater. Phys.* **2001**, *64*, 180406. [[CrossRef](#)]
- Suchanec, G.; Kalanda, N.; Artsiukh, E.; Yarmolich, M.; Sobolev, N.A. Tunneling conduction mechanisms in strontium ferromolybdate ceramics with strontium molybdate dielectric intergrain barriers. *J. Alloys Comp.* **2020**, *860*, 158526. [[CrossRef](#)]
- Takayama, H. Electron-phonon interaction in impure metals. *Z. Phys.* **1973**, *263*, 329–340. [[CrossRef](#)]
- Kondo, J. Resistance minimum in dilute magnetic alloys. *Prog. Theor. Phys.* **1964**, *32*, 37–49. [[CrossRef](#)]
- Matsushita, Y.; Bluhm, H.; Geballe, T.H.; Fisher, I.R. Evidence for charge Kondo effect in superconducting Tl-doped PbTe. *Phys. Rev. Lett.* **2005**, *94*, 157002. [[CrossRef](#)] [[PubMed](#)]
- Hien-Hoang, V.; Chung, N.-K.; Kim, H.J. Electrical transport properties and Kondo effect in $\text{La}_{1-x}\text{Pr}_x\text{NiO}_{3-\delta}$ thin films. *Sci. Rep.* **2021**, *11*, 5391. [[CrossRef](#)] [[PubMed](#)]
- Syskakis, E.; Choudalakis, G.; Papastaikoudis, C. Crossover between Kondo and electron–electron interaction effects in $\text{La}_{0.75}\text{Sr}_{0.20}\text{MnO}_3$ manganite doped with Co impurities? *J. Phys. Condens. Matter* **2003**, *15*, 7735–7749. [[CrossRef](#)]
- Wang, Y.; Xie, C.; Li, J.; Du, Z.; Cao, L.; Han, Y.; Zu, L.; Zhang, H.; Zhu, H.; Zhang, X.; et al. Weak Kondo effect in the monocrystalline transition metal dichalcogenide ZrTe_2 . *Phys. Rev. B Condens. Matter Mater. Phys.* **2021**, *103*, 174418. [[CrossRef](#)]
- Lee, P.A.; Ramakrishnan, T.V. Disordered electronic systems. *Rev. Mod. Phys.* **1985**, *57*, 287–337. [[CrossRef](#)]
- Ziese, M. Searching for quantum interference effects in $\text{La}_{0.7}\text{Ca}_{0.3}\text{MnO}_3$ films on SrTiO_3 . *Phys. Rev. B Condens. Matter Mater. Phys.* **2003**, *68*, 132411. [[CrossRef](#)]
- Suchanec, G.; Artsiukh, E. Absence of weak localization effects in strontium ferromolybdate. *Appl. Sci.* **2023**, *13*, 7096. [[CrossRef](#)]
- Maritato, L.; Adamo, C.; Barone, C.; De Luca, G.M.; Galdi, A.; Orgiani, P.; Petrov, A.Y. Low-temperature resistivity of $\text{La}_{0.7}\text{Sr}_{0.3}\text{MnO}_3$ ultra thin films: Role of quantum interference effects. *Phys. Rev. B Condens. Matter Mater. Phys.* **2006**, *73*, 094456. [[CrossRef](#)]
- Kumar, D.; Sankar, J.; Narayan, J.; Singh, R.K.; Majumdar, A.K. Low-temperature resistivity minima in colossal magnetoresistive $\text{La}_{0.7}\text{Ca}_{0.3}\text{MnO}_3$ thin films. *Phys. Rev. B Condens. Matter Mater. Phys.* **2002**, *65*, 094407. [[CrossRef](#)]
- Herranz, G.; Sánchez, F.; Fontcuberta, J.; Laukhin, V.; Galibert, J.; García-Cuenca, M.V.; Ferrater, C.; Varela, M. Magnetic field effect on quantum corrections to the low-temperature conductivity in metallic perovskite oxides. *Phys. Rev. B Condens. Matter Mater. Phys.* **2005**, *72*, 014457. [[CrossRef](#)]
- Auslender, M.; Kar'kin, A.E.; Rozenberg, E. Low-temperature resistivity minima in single-crystalline and ceramic $\text{La}_{0.8}\text{Sr}_{0.2}\text{MnO}_3$: Mesoscopic transport and intergranular tunneling. *J. Appl. Phys.* **2001**, *89*, 6639–6641. [[CrossRef](#)]
- Kalanda, N.; Demyanov, S.; Yarmolich, M.; Petrov, A.; Sobolev, N. Electric transport characteristics of $\text{Sr}_2\text{FeMoO}_{6-\delta}$ ceramics with structurally inhomogeneous surfaces. In *Workshop Book, Proceedings of the 2nd International Workshop on Advanced Magnetic Oxides (IWAMO), Aveiro, Portugal, 24–25 November 2021*; Department of Physics of the University of Aveiro: Aveiro, Portugal, 2021; p. 24.
- Zhang, J.; Xu, Y.; Yu, L.; Cao, S.; Zhao, Y. Resistivity minimum and the electronic strongly correlation characteristic for $\text{La}_{2/3}\text{Sr}_{1/3}\text{MnO}_3$ thin film. *Physica B* **2008**, *403*, 1471–1473. [[CrossRef](#)]
- Rozenberg, E.; Auslender, M.; Felner, I.; Gorodetsky, G. Low-temperature resistivity minimum in ceramic manganites. *J. Appl. Phys.* **2000**, *88*, 2578–2582. [[CrossRef](#)]
- Barman, A.; Ghosh, M.; Biswas, S.; De, S.K.; Chatterjee, S. Electrical and magnetic properties of $\text{La}_{0.7-x}\text{Y}_x\text{Sr}_{0.3}\text{MnO}_3$ ($0 \leq x \leq 0.2$) perovskite at low temperature. *J. Phys. Condens. Matter* **1998**, *10*, 9799–9811. [[CrossRef](#)]
- Saloaro, M.; Majumdar, S.; Huhtinen, H.; Paturi, P. Absence of traditional magnetoresistivity mechanisms in $\text{Sr}_2\text{FeMoO}_6$ thin films grown on SrTiO_3 , MgO and NdGaO_3 substrates. *J. Phys. Condens. Matter* **2012**, *24*, 366003. [[CrossRef](#)] [[PubMed](#)]

27. Gao, Y.; Cao, G.; Zhang, J.; Habermeier, H.-U. Intrinsic and precipitate-induced quantum corrections to conductivity in $\text{La}_{2/3}\text{Sr}_{1/3}\text{MnO}_3$ thin films. *Phys. Rev. B Condens. Matter Mater. Phys.* **2012**, *85*, 195128. [[CrossRef](#)]
28. Koo, J.H.; Kim, J.-H.; Yu, D.G.; Cho, G. Magnetoresistance in double-perovskite structure for $\text{Sr}_2\text{FeMoO}_6$. *Mod. Phys. Lett. B* **2007**, *21*, 1593–1598. [[CrossRef](#)]
29. Kobayashi, K.I.; Kimura, T.; Sawada, H.; Terakura, K.; Tokura, Y. Room-temperature magnetoresistance in an oxide material with an ordered double-perovskite structure. *Nature* **1998**, *395*, 677–680. [[CrossRef](#)]
30. Nag, A.; Jana, S.; Middley, S.; Ray, S. The many facets of tunneling magnetoresistance in $\text{Sr}_2\text{FeMoO}_6$. *Indian J. Phys.* **2017**, *91*, 883–893. [[CrossRef](#)]
31. Middey, S.; Jana, S.; Ray, S. Surface spin-glass and exchange bias in nanoparticle. *J. Appl. Phys.* **2010**, *108*, 043918. [[CrossRef](#)]
32. Kodama, R.H.; Berkowitz, A.E.; McNiff, E.J., Jr.; Foner, S. Surface spin disorder in NiFe_2O_4 nanoparticles. *Phys. Rev. Lett.* **1996**, *77*, 394–397. [[CrossRef](#)] [[PubMed](#)]
33. Zhu, T.; Shen, B.G.; Sun, J.R.; Zhao, H.W.; Zhan, W.S. Surface spin-glass behavior in $\text{La}_{2/3}\text{Sr}_{1/3}\text{MnO}_3$ nanoparticles. *Appl. Phys. Lett.* **2001**, *78*, 3863–3865. [[CrossRef](#)]
34. Sarma, D.D.; Ray, S.; Tanaka, K.; Kobayashi, M.; Fujimori, A.; Sanyal, P.; Krishnamurthy, H.R.; Dasgupta, C. Intergranular magnetoresistance in $\text{Sr}_2\text{FeMoO}_6$ from a magnetic tunnel barrier mechanism across Grain Boundaries. *Phys. Rev. Lett.* **2007**, *98*, 20157205. [[CrossRef](#)] [[PubMed](#)]
35. Ray, S.; Middey, S.; Jana, S.; Banerjee, A.; Sanyal, P.; Rawat, R.; Gregoratti, L.; Sarma, D.D. Origin of the unconventional magnetoresistance in $\text{Sr}_2\text{FeMoO}_6$. *Europhys. Lett.* **2011**, *94*, 47007. [[CrossRef](#)]
36. Poddar, A.; Bhowmik, R.N.; Muthuselvan, I.P.; Das, N. Evidence of disorder induced magnetic spin glass phase in $\text{Sr}_2\text{FeMoO}_6$ double perovskite. *J. Appl. Phys.* **2009**, *106*, 073908. [[CrossRef](#)]
37. Tomioka, Y.; Okuda, T.; Okimoto, Y.; Kumai, R.; Kobayashi, K.; Tokura, Y. Magnetic and electronic properties of a single crystal of ordered double perovskite. *Phys. Rev. B Condens. Matter Mater. Phys.* **2000**, *61*, 422–427. [[CrossRef](#)]
38. Westerburg, W. Spinpolarisierter Transport in Epitaktischen Manganoxid- und Doppelperowskitschichten. PhD Thesis, Department of Physics in the Johannes Gutenberg-University Mainz, Mainz, Germany, 2000. [[CrossRef](#)]
39. Yanagihara, H.; Salamon, M.B.; Lyanda-Geller, Y.; Xu, S.; Moritomo, Y. Magnetotransport in double perovskite (formula presented) role of magnetic and nonmagnetic disorder. *Phys. Rev. B Condens. Matter Mater. Phys.* **2001**, *64*, 214407. [[CrossRef](#)]
40. Akai, H.; Akai, M.; Blügel, S.; Drittler, B.; Ebert, H.; Terakura, K.; Zeller, R.; Dederichs, P.H. Theory of hyperfine interactions in metals. *Progr. Theor. Phys. Suppl.* **1990**, *101*, 11–77. [[CrossRef](#)]
41. Yarmolich, M.; Kalanda, N.; Demyanov, S.; Fedotova, J.; Bayev, V.; Sobolev, N.A. Charge ordering and magnetic properties in nanosized $\text{Sr}_2\text{FeMoO}_6$ powders. *Phys. Status Solidi B* **2016**, *253*, 2160–2166. [[CrossRef](#)]
42. Thompson, R.S.; Li, D.; Witte, C.M.; Jia, G.; Lu, J.G. Weak localization and electron-electron interactions in indium-doped ZnO nanowires. *Nano Lett.* **2009**, *9*, 3991–3995. [[CrossRef](#)]
43. Hwang, H.Y.; Cheong, S.-W.; Ong, N.P.; Batlogg, B. Spin-polarized intergrain tunneling in $\text{La}_{2/3}\text{Sr}_{1/3}\text{MnO}_3$. *Phys. Rev. Lett.* **1996**, *77*, 2041–2044. [[CrossRef](#)] [[PubMed](#)]
44. Slonczewski, J.C. Conductance and exchange coupling of two ferromagnets separated by a tunneling barrier. *Phys. Rev. B* **1989**, *39*, 6995–7002. [[CrossRef](#)] [[PubMed](#)]
45. Mott, N.F.; Davis, E.A. *Electronic Processes in Non-Crystalline Materials*, 2nd ed.; Clarendon Press: Oxford, UK, 1979.
46. Allub, R.; Alascio, B. Magnetization and conductivity $\text{La}_{1-x}\text{Sr}_x\text{MnO}_3$ -type crystals. *Phys. Rev. B Condens. Matter Mater. Phys.* **1997**, *55*, 14113–14116. [[CrossRef](#)]
47. Efros, A.L.; Shklovskii, B.I. Coulomb gap and low temperature conductivity of disordered systems. *J. Phys. C Solid State Phys.* **1975**, *8*, L49–L51. [[CrossRef](#)]
48. Sheng, P.; Abeles, B.; Arie, Y. Hopping conductivity in granular metals. *Phys. Rev. Lett.* **1973**, *31*, 44–47. [[CrossRef](#)]
49. Niebieskikwiat, D.; Sánchez, R.; Caneiro, A.; Morales, L.; Vásquez-Mansilla, M.; Rivadulla, F.; Hueso, L. High-temperature properties of the double perovskite: Electrical resistivity, magnetic susceptibility, and ESR. *Phys. Rev. B Condens. Matter Mater. Phys.* **2000**, *62*, 3340–3345. [[CrossRef](#)]
50. Zhang, L.; Zhou, Q.; He, Q.; He, T. Double-perovskites $\text{A}_2\text{FeMoO}_{6-\delta}$ ($\text{A} = \text{Ca}, \text{Sr}, \text{Ba}$) as anodes for solid oxide fuel cells. *J. Power Sources* **2010**, *195*, 6356–6366. [[CrossRef](#)]
51. Sheng, P.; Sichel, E.K.; Gittleman, J.I. Fluctuation-induced tunneling conduction in carbon-polyvinylchloride composites. *Phys. Rev. Lett.* **1978**, *40*, 1197–2000. [[CrossRef](#)]
52. Snyder, G.J.; Hiskes, R.; DiCarolis, S. Intrinsic electrical transport and magnetic properties of $\text{La}_{0.67}\text{Ca}_{0.33}\text{MnO}_3$ and $\text{La}_{0.67}\text{Sr}_{0.33}\text{MnO}_3$ MOCVD thin films and bulk material. *Phys. Rev. B Condens. Matter Mater. Phys.* **1996**, *53*, 14434–14444. [[CrossRef](#)] [[PubMed](#)]
53. Schiffer, P.; Ramirez, A.P.; Bao, W.; Cheong, S.-W. Low temperature magnetoresistance and the magnetic phase diagram of $\text{La}_{1-x}\text{Ca}_x\text{MnO}_3$. *Phys. Rev. Lett.* **1995**, *75*, 3336–3339. [[CrossRef](#)]
54. Akimoto, T.; Moritomo, Y.; Nakamura, A.; Furukawa, N. Observation of anomalous single-magnon scattering in half-metallic ferromagnets by chemical pressure control. *Phys. Rev. Lett.* **2000**, *85*, 3914–3917. [[CrossRef](#)] [[PubMed](#)]
55. Dyson, F.J. Thermodynamic behavior of an ideal ferromagnet. *Phys. Rev.* **1956**, *102*, 1230–1244. [[CrossRef](#)]
56. Zhang, H.; Chen, X.J.; Zhang, C.L.; Almasan, C.C.; Habermeier, H.U. Spin-wave scattering at low temperatures in manganite films. *Phys. Rev. B Condens. Matter Mater. Phys.* **2003**, *67*, 134405. [[CrossRef](#)]

57. Kubo, K.; Ohatata, N.A. Quantum theory of double exchange. I. *J. Phys. Soc. Japan* **1972**, *33*, 21–32. [[CrossRef](#)]
58. Urushibara, A.; Moritomo, Y.; Arima, T.; Asamitsu, A.; Kido, G.; Tokura, Y. Insulator-metal transition and giant magnetoresistance in $\text{La}_{1-x}\text{Sr}_x\text{MnO}_3$. *Phys. Rev. B Condens. Matter Mater. Phys.* **1995**, *51*, 14103. [[CrossRef](#)] [[PubMed](#)]
59. Li, G.; Zhou, H.D.; Feng, S.J.; Fan, X.J.; Li, X.G.; Wang, Z.D. Competition between ferromagnetic metallic and paramagnetic insulating phases in manganites. *J. Appl. Phys.* **2002**, *92*, 1406–1410. [[CrossRef](#)]
60. Zhao, G.M.; Smolyaninova, V.; Prellier, W.; Keller, H. Electrical transport in the ferromagnetic state of manganites: Small-polaron metallic conduction at low temperatures. *Phys. Rev. Lett.* **2000**, *84*, 6086–6089. [[CrossRef](#)] [[PubMed](#)]
61. Fisher, B.; Chashka, K.B.; Patlagan, L.; Reisner, G.M. Intergrain tunneling in granular $\text{Sr}_2\text{FeMoO}_6$ studied by pulsed high currents. *Phys. Rev. B Condens. Matter Mater. Phys.* **2003**, *68*, 13442. [[CrossRef](#)]
62. Simmons, J.G. Generalized formula for the electric tunnel effect between similar electrodes separated by a thin insulating film. *J. Appl. Phys.* **1963**, *34*, 1793–1803. [[CrossRef](#)]
63. Helman, J.S.; Abeles, B. Tunneling of spin-polarized electrons and magnetoresistance in granular Ni films. *Phys. Rev. Lett.* **1976**, *37*, 1429–1432. [[CrossRef](#)]
64. Fisher, B.; Genossar, J.; Chashka, K.B.; Patlagan, L.; Reisner, G.M. Remarkable power-law temperature dependencies of inter-grain conductivity. *Solid State Commun.* **2006**, *137*, 641–644. [[CrossRef](#)]
65. Fisher, B.; Genossar, J.; Chashka, K.B.; Patlagan, L.; Reisner, G.M. Intergrain tunnelling in the half-metallic double-perovskites $\text{Sr}_2\text{BB}'\text{O}_6$ ($\text{BB}' = \text{FeMo}, \text{FeRe}, \text{CrMo}, \text{CrW}, \text{CrRe}$). *EPJ Web Conf.* **2014**, *75*, 01001. [[CrossRef](#)]
66. Granville, S.; Farrell, I.L.; Hyndman, A.R.; McCann, D.M.; Reeves, R.J.; Williams, G.V.M. Indications of spin polarized transport in $\text{Ba}_2\text{FeMoO}_6$ thin films. *arXiv* **2017**, arXiv:1707.01208.
67. Sarma, D.D.; Mahadevan, P.; Saha-Dasgupta, T.; Ray, S.; Kumar, A. Electronic structure of $\text{Sr}_2\text{FeMoO}_6$. *Phys. Rev. Lett.* **2000**, *85*, 2549–2552. [[CrossRef](#)] [[PubMed](#)]
68. Mitani, S.; Takahashi, S.; Takanashi, K.; Yakushiji, K.; Maekawa, S.; Fujimori, H. Enhanced magnetoresistance in insulating granular systems: Evidence for higher-order tunneling. *Phys. Rev. Lett.* **1998**, *81*, 2799–2802. [[CrossRef](#)]
69. Haile, S.M.; West, D.L.; Campbell, J. The role of microstructure and processing on the proton conducting properties of gadolinium-doped barium cerate. *J. Mater. Res.* **1998**, *13*, 1576–1595. [[CrossRef](#)]
70. Niebieskikwiat, D.; Prado, F.; Caneiro, A.; Sánchez, R.D. Antisite defects versus grain boundary competition in the tunneling magnetoresistance of the $\text{Sr}_2\text{FeMoO}_6$ double perovskite. *Phys. Rev. B Condens. Matter Mater. Phys. B.* **2004**, *70*, 132412. [[CrossRef](#)]
71. Westerburg, W.; Reisinger, D.; Jakob, G. Epitaxy and magnetotransport of $\text{Sr}_2\text{FeMoO}_6$ thin films. *Phys. Rev. B Condens. Matter Mater. Phys.* **2000**, *62*, R767–R770. [[CrossRef](#)]
72. Venimadhav, A.; Sher, F.; Attfield, J.P.; Blamire, M.G. Oxygen assisted deposition of $\text{Sr}_2\text{FeMoO}_6$ thin films on SrTiO_3 . *J. Magn. Mater.* **2004**, *269*, 101–105. [[CrossRef](#)]
73. Manako, T.; Izumi, M.; Konishi, Y.; Kobayashi, K.-I.; Kawasaki, M.; Tokura, Y. Epitaxial thin films of ordered double perovskite $\text{Sr}_2\text{FeMoO}_6$. *Appl. Phys. Lett.* **1999**, *74*, 2215–2217. [[CrossRef](#)]
74. Liu, G.Y.; Rao, G.H.; Feng, X.M.; Yang, H.F.; Ouyang, Z.W.; Liu, W.F.; Liang, J.K. Metal–semiconductor transition in non-stoichiometric double perovskite $\text{Sr}_2\text{Fe}_x\text{Mo}_{2-x}\text{O}_6$. *Phys. B* **2003**, *334*, 229–233. [[CrossRef](#)]
75. López-Mir, L.; Frontera, C.; Aramberri, H.; Bouzheouane, K.; Cisneros-Fernández, J.; Bozzo, B.; Balcells, L.; Martínez, B. Anisotropic sensor and memory device with a ferromagnetic tunnel barrier as the only magnetic element. *Sci. Rep.* **2018**, *8*, 861. [[CrossRef](#)] [[PubMed](#)]
76. Suchanec, G.; Artiukh, E. Intergranular magnetoresistance of strontium ferromolybdate ceramics caused by spin-polarized tunneling. *Open Ceram.* **2021**, *7*, 100171. [[CrossRef](#)]
77. Suchanec, G.; Artiukh, E.; Gerlach, G. Resistivity and tunnel magnetoresistance in double-perovskite strontium ferromolybdate ceramics. *Phys. Status Solidi B* **2022**, *259*, 2200012. [[CrossRef](#)]
78. Deniz, H.; Preziosi, D.; Alexe, M.; Hesse, D. Coherent Fe-rich nano-scale perovskite oxide phase in epitaxial $\text{Sr}_2\text{FeMoO}_6$ films grown on cubic and scandate substrates. *J. Appl. Phys.* **2017**, *121*, 023906. [[CrossRef](#)]
79. Suchanec, G.; Artiukh, E. Nonstoichiometric strontium ferromolybdate as an electrode material for solid oxide fuel cells. *Inorganics* **2022**, *10*, 230. [[CrossRef](#)]

Disclaimer/Publisher’s Note: The statements, opinions and data contained in all publications are solely those of the individual author(s) and contributor(s) and not of MDPI and/or the editor(s). MDPI and/or the editor(s) disclaim responsibility for any injury to people or property resulting from any ideas, methods, instructions or products referred to in the content.